

**SIMULATION STUDIES AND PRACTICAL TESTS USING MULTI IMAGE SHAPE FROM SHADING<sup>1</sup>**Christian Heipke<sup>(a)</sup>, Christian Piechullek<sup>(b)</sup>, Heinrich Ebner<sup>(c)</sup><sup>(a)</sup> Institut für Photogrammetrie und Ingenieurvermessungen, Universität Hannover, <http://www.ipi.uni-hannover.de><sup>(b)</sup> Axel Springer Verlag, Ahrensburg<sup>(c)</sup> Lehrstuhl für Photogrammetrie und Fernerkundung, Technische Universität München, <http://www.verm.photo.tu-muenchen.de>

Commission III, Working Group III/2

**KEY WORDS:** shape from shading, multiple images, surface reconstruction, real imagery**ABSTRACT**

Multi image shape from shading (MI-SFS) is a surface reconstruction method which has been studied intensively by our group over the last years. Our goal is to develop a method incorporating MI-SFS and image matching for use in planetary science. MI-SFS directly relates the grey values of one or more images to the heights of a digital terrain model (DTM) and the parameters of a radiometric surface model, which describes the surface reflectance behaviour. The DTM heights as well as the parameters of the radiometric model are estimated from the image grey values in a least squares adjustment.

In this paper we shortly review the principles of MI-SFS, and analyse its characteristics using theoretical investigations and a practical example. Throughout the text a comparison of two widely used reflectance models in planetary science, the well-known Lambert and the Lommel-Seeliger reflectance model, is given together with an investigation into the pros and cons of using more than one image and thus of MI-SFS compared to classical SFS. Results from a practical test using digitised aerial images are described, which demonstrate the potential of MI-SFS and its advantages over single image SFS.

**1 INTRODUCTION**

Shape from Shading (SFS) is a method for surface reconstruction from digital images which exploits the fact that surface patches, having different inclination relative to a light source, are imaged with different brightness. The surface is generally assumed to have constant and known reflectance properties. Therefore, SFS only performs well in areas with poor image texture. Using a single digital image, the result is ambiguous because the inclination of a surface patch is determined by two components (e. g. the slopes in x and y direction) while only one observation, namely the grey values of the patch is available. In order to overcome this well known indeterminability of SFS, various constraints were suggested.

SFS has first been suggested by Rindfleisch (1966) and Horn (1970). In the field of astrogeology, where SFS is also referred to as 'photoclinometry' and only few or no stereoscopic images are available, the main research interest lies in the geometric reconstruction of planetary surfaces (e. g. Davis, Soderblom 1984; McEwen 1991; Giese et al. 1996). In computer vision, SFS has been developed for the reconstruction of surfaces in terrestrial and close-range surroundings (e. g. Oren, Nayar 1994; Fua 1997; Lee, Kuo 1997; Wei, Hirzinger 1997). A collection of papers on SFS and a detailed bibliography up to the late eighties is presented in Horn, Brooks (1989), a recent survey of the field is contained in Zhang et al. (1999).

Multi image shape from shading (MI-SFS) is a surface reconstruction method first suggested some time ago (Heipke 1992) and has been studied intensively by our group over the last years (see Piechullek 2000 for a comprehensive description of the work carried out to date). In contrast to classical SFS, MI-SFS is based on perspective transformations between image and object space and directly relates the grey values of one or more images to the heights of a digital terrain model (DTM) and the parameters of a radiometric surface model, which describes the surface reflectance behaviour. The DTM heights as well as the parameters of the radiometric model are estimated from the image grey values in a least squares adjustment. Our goal is to develop a method incorporating MI-SFS and image matching for use in planetary science, e. g. for images from the Mars Express mission which is expected to derive high resolution DTMs from the Martian Surface. Mars Express will be equipped with an updated version of the HRSC camera and is planned to be launched in 2003 (Neukum 1998). The integration of SFS and image matching for this task is advantageous, because the respective prerequisites of both methods are complementary: while SFS needs constant albedo resulting in poor image texture, image matching inherently relies on local grey value differences. In our long term strategy it is planned

---

<sup>1</sup> Most of the work reported in this paper was carried out while all three authors were with the Lehrstuhl für Photogrammetrie und Fernerkundung, Technische Universität München

to first use image matching to create a rough DTM, and to subsequently refine it in areas of constant albedo by means of MI-SFS.

In this paper we shortly review the principles of MI-SFS, and analyse its characteristics using theoretical investigations and a practical example. Throughout the text a comparison of two widely used reflectance models in planetary science, the well-known Lambert and the Lommel-Seeliger reflectance law, is given together with an investigation into the pros and cons of using more than one image and thus of MI-SFS compared to classical SFS.

## 2 MODELS FOR MULTI IMAGE SHAPE FROM SHADING

In order to solve the DTM reconstruction problem by SFS the image formation process has to be modelled and eventually inverted with respect to the parameters describing the object surface. The image grey values are influenced by the radiance and the wavelength of the incident illumination, atmospheric effects, surface reflectance properties, and sensor characteristics. In our approach, the light source is introduced as a distant point light source with known radiometric characteristics. Atmospheric influences are considered to be negligible, and the sensor parameters are assumed to be known from a radiometric and a geometric calibration. Thus, the unknowns of our approach solely relate to the object surface.

Light falls onto the surface enclosing the incidence angle  $i$  between the direction to the light source  $s$  and the local surface normal  $n$  (see figure 1). The incoming irradiance  $E_0$  is partly absorbed and partly scattered back into the upper hemisphere. A sensor lying in direction  $v$  which encloses the emittance angle  $e$  between  $v$  and  $n$  registers the radiance  $L_e$  scattered towards the sensor.

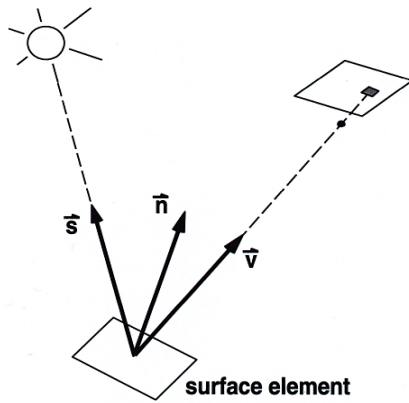


Figure 1: Relationship between direction of illumination  $s$ , surface normal  $n$  and viewing direction  $v$

In our research we have investigated two radiometric models for describing the object surface, the Lambert and the Lommel-Seeliger law. The Lambert law of reflectance is based on the assumption that the brightness of a surface depends only on the incidence angle  $i$  and is thus independent of the emittance angle  $e$ , i. e. the surface looks equally bright from every viewing direction. The Lambert law is widely used in SFS algorithms for its simplicity. It is given by equation (1).

$$r_L(i) = A_L \cos i \quad (1)$$

$A_L$  stands for the Lambertian surface albedo, and  $r_L$  denotes the so called bidirectional reflectance (BDR) which is the ratio between  $L_e$  and  $E_0$ .

In order to extend the assumption that light reflection occurs at the boundary surface between two media only the Lommel-Seeliger law was derived by Seeliger in 1887. In this model light scattering is assumed to take place at individual particles within a layer of infinite thickness below the apparent surface; the radiance observed at a sensor comes from light scattered by all particles in the medium lying within the field of view of the sensor. Therefore, the Lommel-Seeliger law contains not only the incidence angle  $i$  but also the emittance angle  $e$ , see equation (2).

$$r_{LS}(i, e) = A_{LS} \frac{\cos i}{\cos i + \cos e} \quad (2)$$

This law is a good description of the light scattering behaviour of low-albedo surfaces (see also Piechullek, Heipke 1996), in contrast to the Lambert law, which is more valid for bright surfaces. Some of the most sophisticated reflectance models widely used in planetary photometry to derive specific information of the surface material (e.g. Hapke 1993) are extensions of the Lommel-Seeliger law.

In figures 2 and 3 the two reflectance models are depicted graphically with respect to the incidence and emittance angle. From the figures and the equations it can be seen that for the Lommel-Seeliger model for a vertical image of a horizontal surface patch ( $e = 0$ ) with illumination directly from above ( $i = 0$ )  $r_{LS}$  is only half the value of  $r_L$ . This is the reason why in combined models such as the Lunar-Lambert model (McEwen 1991) the Lommel-Seeliger term is introduced with a factor of 2 as compared to the Lambert term. This factor is also included into the following derivations, and a subscript for the albedo is omitted.

In order to appropriately describe the object space, a geometric and a radiometric surface model are introduced. These models have also been employed in the global image matching approaches in object space (Heipke 1990; Holm 1999). The geometric model consists of a grid DTM. The grid is defined in the XY-plane of the object surface with grid nodes  $X_k, Y_l$  and corresponding grid heights  $Z_{kl}$ . The mesh size of the grid depends on the roughness of the terrain. A height  $Z$

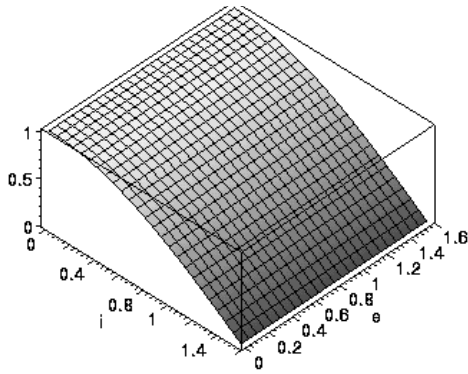


Figure 2: The Lambert reflectance model

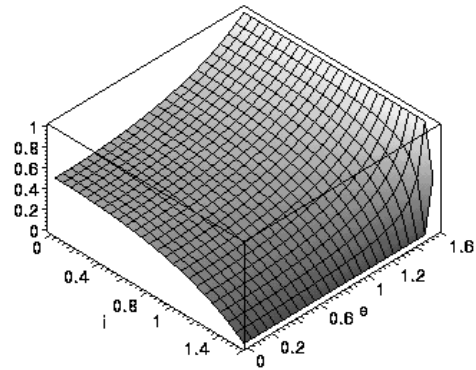


Figure 3: The Lommel-Seeliger reflectance model

at an arbitrary point is interpolated from the neighbouring grid heights, e. g. by bilinear interpolation. At each point of the object surface the surface normal vector  $n$  thus becomes a function of the neighbouring  $Z_{kl}$ .

In the radiometric model a uniform albedo  $A$  is assigned to the object surface. Object surface elements of constant size are defined within each grid mesh. The size is chosen approximately equal to the pixel size multiplied by the average image scale factor. Assuming known parameters for the exterior orientation and thus known components of the vector  $v$  model grey values denoted by  $G_L$  and  $G_{LS}$ , respectively, can be assigned to each object surface element.  $G_L$  and  $G_{LS}$  can be equated with the corresponding BDR values  $r_L$  and  $r_{LS}$ , and can thus be related analytically to the surface albedo  $A$ , the surface normal  $n$ , and to the DTM heights  $Z_{k,l}$ :

$$G_L = r_L = A \cos(\vec{n}(Z_{k,l}), \vec{s}) \quad (3)$$

$$G_{LS} = r_{LS} = 2 A \frac{\cos(\vec{n}(Z_{k,l}), \vec{s})}{\cos(\vec{n}(Z_{k,l}), \vec{s}) + \cos(\vec{n}(Z_{k,l}), \vec{v})} \quad (4)$$

If also the direction of illumination  $s$  is assumed to be known, the only unknown quantities in the equations (3) and (4) are the parameters of the object surface models, the DTM heights  $Z_{kl}$  and the surface albedo  $A$ . For each image  $j$  with given interior orientation parameters the considered object surface element can be projected into image space using the well known collinearity equations, and image grey values  $g_j$  can be resampled from the original grey values at this position. The  $g_j$  are considered as observations in a least squares adjustment for the estimation of the unknowns. The corresponding observation equations read (omitting the indices L and LS for the model grey values to arrive at a common notation for both reflectance models):

$$v_j = G_j(A, Z_{k,l}) - g_j(Z_{k,l}) \quad (5)$$

$v_j$  stands for the residuals of the adjustment. Since equation (5) is non-linear with respect to the  $Z_{kl}$ , an iterative computational scheme is needed, and initial values for the object space parameters must be available. In equation (6) the structure of the linearised observation equations is given.

$$v_j = (\partial G / \partial Z_{k,l} - \partial g / \partial Z_{k,l}) \Delta Z_{k,l} + \partial G / \partial A \Delta A - (g_j - G_j)_0 \quad (6)$$

$\Delta Z_{k,l}$  and  $\Delta A$  are the changes of the unknowns from iteration to iteration, and  $(g_j - G_j)_0$  is the difference between the image and the model grey value computed from the initial values for the unknowns.

If two or more images taken from different viewpoints are given, stereoscopic correspondence between DTM meshes projected into the images is implicitly exploited, and therefore absolute heights can be computed. The model can also be used if only one single image is available. In this case the classical indeterminability of SFS is overcome by the introduction of the geometric surface model which stabilises the solution. However, only height differences rather than absolute heights can be derived, because from a single image an image scale factor cannot be determined. In order to obtain absolute heights, it is sufficient to consider one of the DTM heights as constant.

While MI-SFS generalises classical SFS by allowing for a perspective transformation between image and object space, and for the simultaneous processing of multiple images, it shares some of the assumptions often found in SFS approaches. Interreflections and self shadowing are not modelled, and the object surface must have constant albedo and must be piecewise smooth without breaklines. Also, occlusions are not accounted for in the model.

### 3 THEORETICAL ANALYSIS OF MULTI IMAGE SHAPE FROM SHADING

In order for this method to work noticeable local grey value gradients  $\partial g / \partial Z$ ,

$$\partial g / \partial Z_{k,l} = \partial g / \partial r \partial r / \partial Z_{k,l} + \partial g / \partial c \partial c / \partial Z_{k,l} \quad (7)$$

in line with the employed reflectance model must be available in image space ( $r$  and  $c$  stand for the pixel coordinates row and column). Otherwise, the matrix of normal equations within the least squares adjustment will become singular. While this condition is the same for least squares image matching and MI-SFS, it is more critical in the case discussed here due to the generally poor texture in areas suitable for SFS, i. e. areas with constant albedo. As can be seen from equation (7) this condition has two important implications: (1) a shift in the DTM heights  $Z_{kl}$  must result in a noticeable shift in image space, i.e.  $\partial r / \partial Z$  or  $\partial c / \partial Z$  must be noticeable, and (2) such a shift must in turn result in noticeable local grey value difference  $\partial g / \partial r$  and  $\partial g / \partial c$  between the neighbouring pixels.

A number of restrictions follow from this condition when applying the proposed method to a planetary scenario:

- (1) Planar surfaces cannot be reconstructed. In the Lambert law the BDR only depends on the incidence angle  $i$  which is constant for the whole plane. Thus, all images of this plane have uniform brightness,  $\partial g / \partial r$  and  $\partial g / \partial c$  are both zero. The situation is somewhat better for the Lommel-Seeliger law, because the BDR also depends on the emittance angle  $e$ . However, for all realistic planetary applications due to the small instantaneous field of view of the employed sensors neighbouring pixels will have nearly the same emittance angle, and thus nearly the same grey value. Again, no local grey values are present.
- (2) Undulated surfaces, on the other hand can be reconstructed from one or multiple images. However, in case only one vertical image is available, i. e. the optical axis is more or less parallel to the Z-axis of the object coordinate system, areas near the nadir point can create problems regardless of the employed reflectance model, because  $\partial r / \partial Z$  and  $\partial c / \partial Z$  might be both too small. This problem can be resolved by changing the direction of the axes of the object coordinate system.
- (3) A small incidence angle  $i$  will generate only small grey value gradients (see figure 2 and 3) and can create problems for the Lambert case, especially if only one image is available and stereoscopic correspondence cannot be used. For the Lommel-Seeliger case this issue occurs as well, but can be at least partly solved by choosing a large emittance angle  $e$ . If possible a large incidence angle should be used.
- (4) The BDR for Lommel-Seeliger type surfaces is relatively flat (see again figure 3), especially for values of  $i$  and  $e$  being similar and below approximately 60 degrees. If both angles are identical the BDR even becomes independent of  $i$  and  $e$ , and thus of the terrain inclination, and takes on the value of  $0.5 A_{LS}$  (see equation 2). Thus, when the emittance angle can be influenced a value different from the incidence angle and as large as possible should be chosen.
- (5) Since the BDR depends linearly on the albedo (see equations 1 and 2) surfaces should be imaged with as much irradiance as possible, i. e. with as large an exposure time as possible.
- (6) Radiometric manipulations of the images will have different results with respect to the resulting surface shape. A constant change in overall surface brightness (offset) will primarily change the estimated surface albedo, but the normal vectors will also be effected. A positive offset will lead to smaller variations of the surface normal, a negative offset will lead to larger ones. A linear change in surface contrast (gain factor) on the other hand will have no effect, because the resulting linear contrast enhancement will be completely compensated for by the estimated surface albedo. Brightness and contrast enhancement of individual images, however, can have unpredictable effects.
- (7) Due to the generally poor image texture, noise can be a particularly difficult problem for the Lambert and the Lommel-Seeliger case. In order to reduce the noise level it is advisable to filter the images using a lowpass prior to the surface reconstruction.

In extensive simulation studies (Piechullek et al. 1998; Piechullek 2000) all mentioned points were verified. While the points (1) to (6) follow directly from the given equations, the influence of noise was investigated in more detail. Three error-free synthetic images from different viewpoints were generated using an undulated terrain. Using these error-free images stable results for the object surface were achieved with a range of different DTMs as initial values for the unknown heights. Subsequently, the images were contaminated by Gaussian noise with a standard deviation of 6 grey values. While the results obtained from these noisy images were clearly a function of the DTM used as initial values, lowpass-filtering and thus noise reduction prior to surface reconstruction produced the desired results: convergence towards the correct result was again achieved. The radius of convergence was found to be approximately 20 pixels for both, the Lambert and the Lommel-Seeliger case. A comparison between the results from the error-free and the noisy, filtered images revealed that the effect of filtering onto the geometric accuracy of the reconstruction was negligible.

The simulations were also carried out for individual images. As was to be expected, in this case the accuracy of the obtained results was worse by a factor of about 2 compared to the solution with three images due to the lower redun-

dancy. Another result from this comparison was that while with individual images the problems described in points (2), (3) and (4) could all be found and partly prevented a correct solution to be obtained, in the simultaneous solution with all three images these problems could be overcome. This finding proves that the simultaneous solution besides offering more redundancy, is also more stable. The main reason for this stability is seen in the exploitation of the stereoscopic correspondence and thus the ray intersection in object space.

## 4 EXPERIMENTAL INVESTIGATIONS USING REAL IMAGERY

### 4.1 Test goal, input data and image pre-processing

The goal of these investigations was to demonstrate the potential of MI-SFS for surface reconstruction using real images. Since no appropriate test images acquired directly in digital form were available we used digitised aerial film images. Some image pre-processing (see below) was necessary since no information about the photographic treatment of the analogue images could be obtained. By comparing the result of the surface reconstruction to an analytically measured reference DTM we wanted to prove that the proposed MI-SFS method has the potential of accurately reconstructing a surface of constant albedo. Finally the radius of convergence of MI-SFS was to be determined in the same way as in the mentioned simulation studies.

For the tests three black and white aerial images with an image scale of approximately 1:10.000 of an image strip taken with a wide angle camera were used (for the set up of the images see figure 4). The images show a homogeneous, poorly textured sand dune area in Eastern Arabia. The interior and exterior orientation were determined using an analytical plotter, the images were subsequently digitised with a pixel size of  $30 \times 30 \mu\text{m}^2$  resulting in a ground sample resolution of about  $0.3 \times 0.3 \text{ m}^2$ . The images of the test area (see figure 5) are about  $512 \times 512$  pixels in size and contain very poor texture and only small grey value differences. The illumination direction was calculated from the known time of the image acquisition and the geographical coordinates of the imaged surface area.

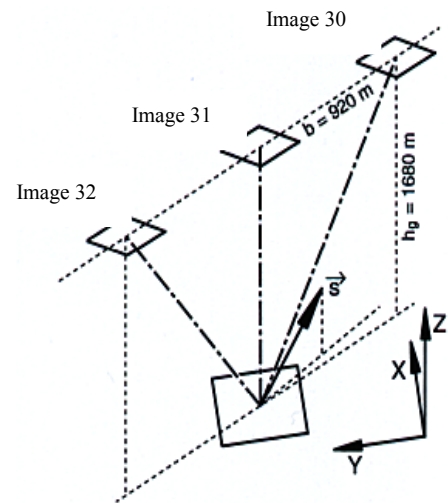


Figure 4: Geometric situation of image acquisition and illumination, real images

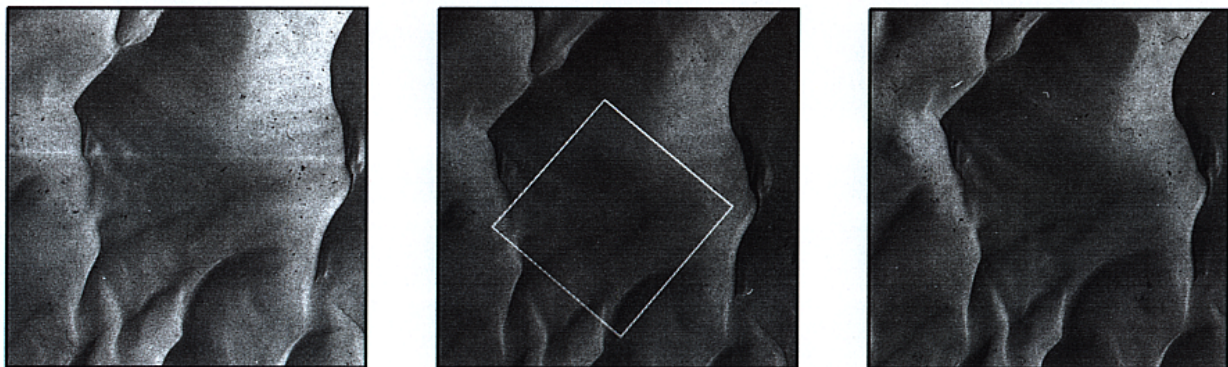


Figure 5: Real images no. 30, 31, and 32. In image no. 31 the area being processed is depicted as a white square

The chosen test area lies in one of the sand dune flanks, where smooth surface undulations, but no edges are present. The maximum height difference within the area is about 10 meters. For this area, a DTM grid of  $35 \times 35$  heights with a mesh size of 2.4 m was measured analytically (see figure 6). Each DTM grid height was measured twice and independently, resulting in a root mean square value for the averaged DTM heights of 0.32 m. The geometric and the radiometric model used in MI-SFS were chosen in correspondence with the analytically measured DTM: the grid size was set to 2.4 m and the size of the object surface element to  $(0.3 \text{ m})^2$ . Thus, each grid mesh contained  $8 \times 8$  object surface elements. The gradients  $\partial r / \partial Z$  and  $\partial c / \partial Z$  in image space amounted to about 1 to 2 pixels/m. Due to the lack of radiometric ground truth or independent reflectance measurements, no information was available about the reflectance properties of the imaged surface.

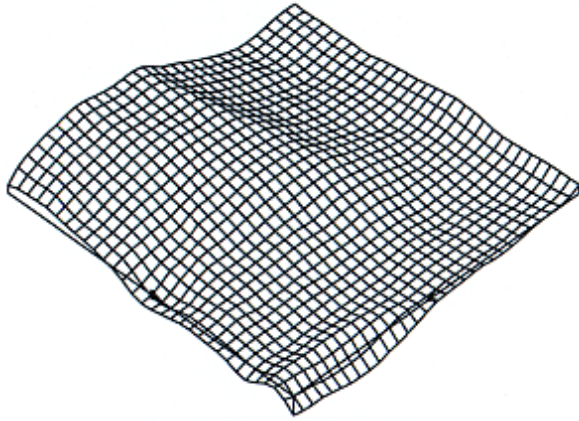


Figure 6: Perspective view of the reference DTM

images were subsequently compared to their real counterparts in order to determine the parameters of a linear grey-value transformation for each image by a least-squares fit, and this linear transformation was then applied to the real images. Polynomials of higher order were also tested, but they did not improve the results in terms of the least-squares fit. Finally, these images were filtered using a Gaussian lowpass in order to reduce any image noise.

#### 4.2 Surface reconstruction

The images thus pre-processed were used in the described MI-SFS approach. Experiments were conducted with a varying number of images, each time using either the Lambert law or the Lommel-Seeliger law with a horizontal plane at an average height within the test area as initial DTM. The rationale for the selection of the initial values comes from our long term strategy in which a rough DTM is assumed to be available prior to employing MI-SFS. Convergence of the iterative computations was postulated when each change in height from one iteration to the next was below 0.1 m. The results were then compared to the reference DTM. In this comparison the two parameters  $Z_0$  (offset) and  $m$  (scale factor) of a linear transformation were computed, and the root mean square error  $s(\Delta Z)$  and the maximum absolute deviation  $\Delta Z_{\max}$  of the two surfaces after applying this transformation was determined (see table 1).

The results can be summarised as follows:

- When comparing the results of the multi image processing given in table 1 it becomes clear that the reflectance properties of the investigated surface are better approximated by the Lambert law. Therefore, the results of the Lommel-Seeliger runs with the individual images are omitted from the table.
- The accuracy of the obtained results in terms of  $s(\Delta Z)$  amounts to 0.43 m. This value still contains the accuracy of the reference DTM (0.32 m), and is equivalent to 0.3‰ of the flying height. Considering the poor image texture, this result can be said to fulfil the expectations.

Image number(s)	$Z_0$ [m]	M	$\Delta Z_{\max}$ [m]	$s(\Delta Z)$ [m]
<b>Lambert reflectance model</b>				
30, 31, 32	-0.10	1.01	1.49	0.43
30	0.09	0.74	4.74	1.72
31	0.36	0.75	15.87	2.49
32	0.57	0.33	19.84	3.83
<b>Lommel-Seeliger reflectance model</b>				
30, 31, 32	0.40	0.85	3.84	1.36

Table 1: Results of the practical test

- Some small deviations remain after the computations. For this result no single source of error can be given. Possible explanations relate to the object surface characteristics: there is obviously no guarantee that (1) the employed Lambert law is valid throughout the whole surface, and (2) that the albedo is in fact spatially constant. From our experience with the different reflectance laws small deviations from the Lambert law do not influence the results in the observed extend. Thus, local albedo variations seem to be the most probable reason for the small observed deviations.

Between the individual original film images distinct differences in contrast and brightness are noticeable (see again figure 5). These differences are larger than effects which can be explained with respect to different view-points in conjunction with commonly used reflectance models such as the Lambert or the Lommel-Seeliger law, and they can significantly influence the MI-SFS results (see discussion on radiometric manipulations in chapter 3). The most probable cause for these differences lies in the photographic processing applied to the analogue photographs. Unfortunately, we had no knowledge of this process. Therefore, we had to approximate the related effects mathematically in an image pre-processing step. First, an average albedo value was estimated from the digital images by considering the analytically measured DTM as constant within our MI-SFS algorithm. The determined albedo, together with the analytically measured DTM, was then used to generate synthetic images. These

- The results of processing the images individually were significantly worse. This result demonstrates convincingly the advantages of MI-SFS over single image SFS. Both, the implicit stereoscopic correspondence of the DTM meshes and the higher redundancy of the whole adjustment contribute to this finding (see also discussion at the end of chapter 3). It must be mentioned, however, that the pre-processing step – more precisely the estimation of the albedo - was designed for the simultaneous processing of all three images. Thus, the pre-processed images individually do not necessarily represent the correct grey values of the object surface any more.

In an additional set of experiments the radius of convergence using the real images was found to be about 16 pixels which is in line with the simulation results (see again chapter 3). In these experiments the analytically measured DTM was changed in absolute height by an offset value and in form by introducing a scale factor. In most cases the surface form was reconstructed within only a few iterations, and for the absolute heights to converge towards the correct result up to 30 iterations were needed.

## 5 CONCLUSIONS

The reported MI-SFS results obtained from the simultaneous evaluation of the radiometrically pre-processed images clearly demonstrate the applicability of the method to real imagery. DTM heights were determined from aerial images of poor texture with a standard deviation of 0.3% of the flying height. Also the advantages of MI-SFS over single image SFS could be proven. They consist in (1) the possibility to directly compute absolute DTM heights as opposed to inclinations and thus height differences, (2) more reliable results in situations in which single image SFS can become numerically unstable, e. g. in the presence of noise, for small incidence angles or for similar values for incidence and emittance angle (the latter only for the Lommel-Seeliger law).

However, the results with real images were only achieved after pre-processing the images. In this pre-processing step the DTM heights of the object surface to be computed were already needed. The reason for this pre-processing was the presence of significant brightness and contrast differences, larger than those which can be explained with respect to different viewpoints in conjunction with commonly used reflectance models in planetary science. It was therefore assumed that these brightness and contrast differences stem from the photographic handling of the analogue images. Given this assumption and the fact that the photographic handling cannot be modelled adequately, MI-SFS could not be independently assessed with the used experimental data, rather only the potential of the method could be proven. One could have also attempted to simultaneously solve for the parameters of the pre-processing and the DTM heights. In this case a brightness offset and a contrast factor would have had to be considered for each image individually, and the unknown surface albedo would have had to be introduced as a constant value, since image contrast and surface albedo are linearly dependent. However, such an approach would have weakened the adjustment model and was not pursued.

In spite of the mentioned shortcomings of the used experimental data, the presented results demonstrate the general applicability of MI-SFS, and in particular its advantages when compared to single image SFS: absolute heights can be derived rather than surface slopes only, the stereoscopic correspondence adds significantly to obtaining stable results, and the higher redundancy renders the result more robust with respect to noise and blunders. Possible extensions of the method include the introduction of another viewing geometry, e. g. the 3-line geometry of HRSC employed on the planed Mars Express mission, the use of a more refined reflectance model, e. g. the Lunar-Lambert model, the consideration of spatially varying albedo, and the introduction of multispectral imagery. In the latter case each spectral band has to be modelled individually as far as the radiometric model is concerned, however, the geometric model remains the same for all spectral bands. As a final note it must be mentioned that a conclusive evaluation of MI-SFS can only be on directly acquired digital imagery from a radiometrically calibrated sensor.

## 6 REFERENCES

Davis, P. A., Soderblom, L. A. (1984): Modeling Crater Topography and Albedo From Monoscopic Viking Orbiter Images; 1. Methodology, *Journal of Geophysical Research* (89) B11, 9449—9457.

Fua, P. (1997): From Multiple Stereo Views to Multiple 3-D Surfaces, *International Journal of Computer Vision*, (24) 1, 19-35.

Giese, B., Oberst, J., Kirk, R. L., Zeitler, W. (1996): The Topography of Asteroid Ida: A Comparison Between Photogrammetric and Two-Dimensional Photoclinometric Image Analysis, *International Archives for Photogrammetry and Remote Sensing* (31) B3/III, 245—250.

Hapke, B. (1993): *Theory of Reflectance and Emittance Spectroscopy*. Topics in Remote Sensing III, Cambridge University Press, Cambridge, Massachusetts.

- Heipke, C. (1990): Integration von Bildzuordnung, Punktbestimmung, Oberflächenrekonstruktion und Orthoprojektion innerhalb der digitalen Photogrammetrie, DGK-C 366.
- Heipke C., 1992: Integration of digital image matching and multi image shape from shading, in: Fuchs S., Hoffmann R. (Eds.), Mustererkennung 1992, Proceedings 14. DAGM Symposium, Informatik aktuell, Springer, Berlin, 186-198.
- Holm M. (1999): Some quality aspects of global object reconstruction, *Surveying Science in Finland* (17), 1-2, 54-64.
- Horn, B. K. P. (1970): Shape from Shading: A Method for Obtaining the Shape of a Smooth Opaque Object from One View, Dissertation, Department of Electrical Engineering, MIT, Cambridge, Massachusetts.
- Horn B.K.P., Brooks M.J. (Eds., 1989): Shape from Shading, The MIT Press, Cambridge, Massachusetts.
- Lee, K. M., Kuo, C.-C. J. (1997): Shape from Shading with a Generalized Reflectance Map Model, *Computer Vision and Image Understanding*, (67) 2, 143—160.
- McEwen, A. S. (1991): Photometric Functions for Photoclinometry and Other Applications, *Icarus*, (92), 298—311.
- Neukum G. (1998): High resolution stereo camera HRSC on the Mars Express Orbiter, Proposal to the European Space Agency, Institut für Planetenerkundung, DLR Berlin-Adlershof.
- Oren, M., Nayar, S. K. (1994): Seeing Beyond Lambert's Law, in: Eklundh, J.-O. (Ed.) *Lecture Notes in Computer Science: Computer Vision - ECCV '94*, (800) 2, Springer, 269-280.
- Piechullek, C., Heipke, C. (1996): DTM Refinement Using Multi Image Shape from Shading, *International Archives of Photogrammetry and Remote Sensing* (31) B3/III, 644—651.
- Piechullek, C., Heipke, C., Ebner, H. (1998): Multi Image Shape from Shading - Results Using Real Aerial Imagery, *International Archives of Photogrammetry and Remote Sensing* (32) 3/1, 160—167.
- Piechullek, C. (2000): Oberflächenrekonstruktion mit Hilfe einer Mehrbild-Shape-from-Shading-Methode, DGK-C 518.
- Rindfleisch, T. (1966): Photometric Method for Lunar Topography, *Photogrammetric Engineering* (32) 2, 267—277.
- Wei, G.-Q., Hirzinger, G. (1997): Parametric Shape-from-Shading by Radial Basis Functions, *IEEE Transactions on Pattern Analysis and Machine Intelligence* (19) 4, 353—365.
- Zhang, R., Tsai, P.-S., Cryer, J. E., Shah, M. (1999): Shape from Shading: A Survey, *IEEE Transactions on Pattern Analysis and Machine Intelligence* (21) 8, 690—706.